This is a repository copy of *Electrical properties of calcia-stabilised zirconia ceramics : voltage-induced p-type conductivity and oxygen redox activity*.

White Rose Research Online URL for this paper:
https://eprints.whiterose.ac.uk/174578/

Version: Published Version

Article:
Ramírez-González, J. and West, A.R. orcid.org/0000-0002-5492-2102 (2021) Electrical properties of calcia-stabilised zirconia ceramics : voltage-induced p-type conductivity and oxygen redox activity. Open Ceramics, 6. 100117.

https://doi.org/10.1016/j.oceram.2021.100117

Reuse
This article is distributed under the terms of the Creative Commons Attribution-NonCommercial-NoDerivs (CC BY-NC-ND) licence. This licence only allows you to download this work and share it with others as long as you credit the authors, but you can't change the article in any way or use it commercially. More information and the full terms of the licence here: https://creativecommons.org/licenses/

Takedown
If you consider content in White Rose Research Online to be in breach of UK law, please notify us by emailing eprints@whiterose.ac.uk including the URL of the record and the reason for the withdrawal request.

eprints@whiterose.ac.uk
https://eprints.whiterose.ac.uk/

Open Ceramics 6 (2021) 100117

Contents lists available at ScienceDirect

Open Ceramics

journal homepage: www.editorialmanager.com/oceram

Electrical properties of calcia-stabilised zirconia ceramics: Voltage-induced *p*-type conductivity and oxygen redox activity

Julia Ramírez-González *, Anthony R. West *

Department of Materials Science and Engineering, The University of Sheffield, Mappin Street, Sheffield, S1 3JD, UK

ARTICLE INFO

Keywords:
Calcia-stabilised zirconia
Impedance spectroscopy
p-type conductivity
Oxygen redox activity

ABSTRACT

The electrical properties of oxide ion-conducting $Ca_{0.15}Zr_{0.85}O_{1.85}$, CSZ, ceramics were investigated using impedance spectroscopy as a function of temperature and applied *dc* bias. The total resistance showed a time-dependent decrease during application of a *dc* bias and was attributed to the reversible introduction of *p*-type semiconductivity, initially at the sample surface followed by grain boundaries and the sample bulk. Electron holes may be located on under-bonded oxygen ions which are associated either with Ca dopant ions or the ceramic surfaces and interfaces, resulting in mixed oxide ion and *p*-type electronic conduction. This *p*-type behaviour with a *dc* bias is different from the behaviour of most well-studied, stabilised zirconias which become *n*-type mixed conducting due to oxygen loss at low pO_2.

1. Introduction

Cubic stabilised zirconias such as yttria-stabilised YSZ and calcia-stabilised CSZ are well-known oxide ion conductors [1]. The limits of their electrolytic domain, Fig. 1, have been studied, especially with evidence of *n*-type conduction at low pO_2 associated with oxygen loss and electron injection into samples. Although it is expected that these zirconias would also show the opposite behaviour at high pO_2 associated with the onset of *p*-type conductivity, there are few well-documented reports of its occurrence, possibly because of the difficulty in accessing a suitable, wide range of high pO_2 values. The possibility of *p*-type conduction in CSZ was predicted at very high pO_2 [2] but has not been confirmed experimentally. In YSZ, *p*-type conductivity was shown by impedance measurements in atmospheres of varying pO_2, but only in compositions with high yttria content [3] and not in compositions such as YSZ8 which are the most widely studied and used for various applications.

Impedance measurements made at the same time as a *dc* bias is applied can provide information on Schottky barriers [4] and help to distinguish between material-based impedances and those associated with potential barriers. They can also give information on the current carriers in a sample produced as a result of field-induced ionisation processes [5–10]. For example, it was shown that *p*-type semi-conductivity was induced in ceramics of YSZ8 under the action of a *dc* bias as small as 1 V which increased to the extent that, at 556 °C and with a field of 43 Vcm^{-1}, a transport number of approximately 0.5 was obtained for both the electronic and oxide ion conducting components [10]. Many of the applications of fluorite-based oxides, such as solid electrolytes in fuel cells and oxygen sensors, depend on an oxide ion transport number of unity and therefore, the effects of a *dc* bias can have practical consequences for the accuracy of measurements as well as acting as a source of valuable scientific information.

The occurrence of *p*-type conductivity in ceramic oxides under certain circumstances is widely recognised although there is little general discussion about the possible location of the holes. Given that the *p*-type conductivity is usually thermally-activated, the holes must be located on atomic species rather than delocalised in a band structure. In a material such as YSZ or CSZ, it is not realistic to expect the holes to be located on Zr, Y or Ca since these are already present in their maximum valence states. Unless unavoidable redox-active impurity ions are present, and in sufficient concentration to give rise to measurable *p*-type conductivity, the unavoidable conclusion is that the holes are located on oxygen, giving rise to O^- ions [5–10].

As far as we are aware, the only examples of *p*-type conductivity in zirconia-based oxides, that has been attributed to holes located on oxygen, are for YSZ8 [9,10] in response to application of a *dc* bias and Y-rich YSZ compositions such as YSZ50 in response to both a *dc* bias and changing pO_2 [3]. Given the general importance of this phenomenon, it is important to establish how widespread it may be and the conditions/materials in which it may occur. Here we report a first study on

* Corresponding authors.
E-mail addresses: jramirezgonzalez1@sheffield.ac.uk (J. Ramírez-González), a.r.west@sheffield.ac.uk (A.R. West).

https://doi.org/10.1016/j.oceram.2021.100117
Received 4 March 2021; Received in revised form 28 April 2021; Accepted 3 May 2021
Available online 7 May 2021
2666-5395/© 2021 The Author(s). Published by Elsevier Ltd on behalf of European Ceramic Society. This is an open access article under the CC BY-NC-ND license (http://creativecommons.org/licenses/by-nc-nd/4.0/).

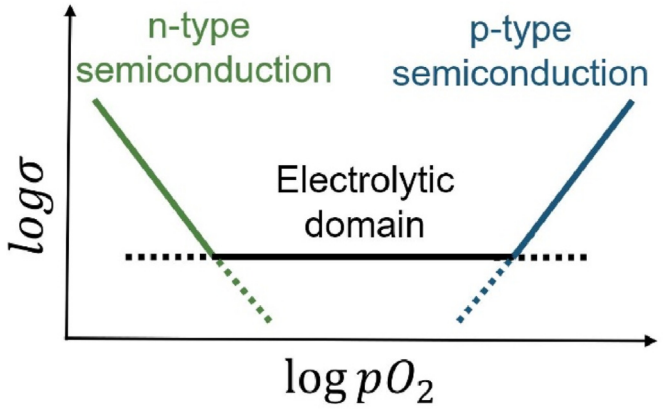

Fig. 1. Conductivity (σ) as a function of oxygen partial pressure (pO_2).

CSZ and choose one composition, CSZ15, which lies in the range of stabilised cubic solid solutions. It does, indeed, show evidence of *p*-type conductivity, attributable to holes on oxygen, in addition to the majority, oxide ion conductivity.

2. Experimental

Samples with composition $Ca_xZr_{1-x}O_{2-x}$: x = 0.15 (CSZ15) were prepared by solid-state reaction using $CaCO_3$ (99%, Fisher) and ZrO_2 (99%, Aldrich), which were dried overnight at 180 and 1000 °C respectively, as described previously [11]. Stoichiometric amounts of reagents were weighed on a Sartorius Entris balance with a tolerance of ±0.0003 g. The mixtures were ground manually with acetone using a pestle and mortar and heated in alumina crucibles at 1150 °C overnight to decarbonate the $CaCO_3$ and start the reaction. Next, the powders were reground, pressed uniaxially into pellets of 10 mm diameter at around 98 MPa and sintered for 10 h at 1600 °C, by taking the CaO–ZrO_2 phase diagram as reference [12], with a heating and cooling rate of 5 °C/min. Pellet densities were ~93%. Pt paste electrodes were applied to opposite pellet faces and dried at 900 °C for 2 h, for impedance measurements. X-ray diffraction patterns of crushed pellets were obtained using a STOE STADI P diffractometer (Darmstadt, Germany), Cu $K\alpha_1$ radiation. The data were collected over 2θ = 20–80° and compared to the diffraction pattern of cubic zirconia (PDF card = 01-070-7361) using the JCPDS database. The results, previously reported [11], confirmed completion of reaction and the formation of a cubic, stabilised zirconia solid solution.

For impedance measurements, electroded pellets were attached to the Pt leads of an in-house conductivity jig with the facility to vary the atmosphere flowing over the pellet. Gases were dried by directing the flow through a desiccator to avoid the possibility of water absorption and proton conduction. Impedance measurements were taken between 350 and 850 °C using two impedance analysers: a Modulab XM MTS (measurement accuracy ±0.1%), frequency range 100 mHz–1 MHz and an Agilent 4294A (measurement accuracy ±0.08%), frequency range 40 Hz-1 MHz, with a nominal *ac* voltage of 100 mV in both cases. In some measurements, a *dc* bias in the range 0.5–25 V was applied across samples, using the dc bias mode, at the same time as impedance data were recorded.

The *dc* bias and temperature cut-off profiles are shown in Fig. 2. The aim was to register any changes to, or recovery of, the sample both during application of a voltage and after its removal. In this set of experiments, impedance measurements were taken at a constant temperature. Two sets of corrections were made to the collected data: (i) a geometric factor concerning pellet thickness and sample-electrode contact area and (ii) jig characteristics consisting of the blank, open circuit capacitance, typically 6 pF and the closed circuit resistance of, primarily, the leads, 1–2 Ω. No correction to the grain boundary impedance values was made, partly because of uncertainty over the grain boundary geometry. Resistance

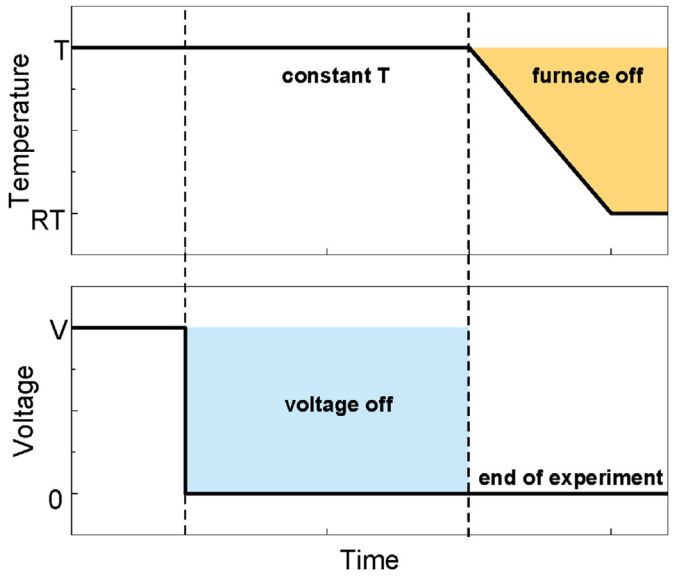

Fig. 2. Temperature and dc bias cut-off profile.

data are therefore reported in resistivity units of ohm cm, even though the grain boundary values are corrected only for overall sample geometry. Data analysis and equivalent circuit fitting was performed using ZVIEW software (ZVIEW-Impedance Software version 3.5f Scribner Associates).

For microstructural and elemental analysis, fracture surfaces of CSZ15 pellets were analysed. The samples were mounted on aluminium stubs with Ag paste and sputter coated with 10 nm of carbon. Scanning electron microscopy (SEM) images were taken on a field-emission scanning electron microscope (FEI Inspect F50) using an acceleration voltage of 15 kV and energy-dispersion analysis of X-rays (EDX) from Oxford Instruments using 20 kV.

3. Results

3.1. Low temperatures and voltages; 0.5–8 V at 391 °C

The impedance response of $Ca_{0.15}Zr_{0.85}O_{1.85}$ without voltage application at 391°C shows 3 elements, Fig. 3 (black line). The Z* plane (a) presents, with decreasing frequency, 2 semicircles and a 45° inclined spike. Replotting the same data as a spectroscopic plot of capacitance vs frequency (b) shows three regions, two with almost constant capacitances of ~2 $pFcm^{-1}$ at high frequencies and ~ 0.5 $nFcm^{-1}$ at intermediate frequencies, and at low frequency, a dispersion reaching ~ 0.3 μFcm^{-1}. These capacitance values are typical of bulk, grain boundary and sample-electrode interface impedances, respectively. The presence of a high capacitance, sample-electrode interface is usually taken as indication of ionic conductivity and for the case of cubic zirconias, this is attributed to oxide ions [13].

Seven sets of impedance measurements were then taken sequentially at the same temperature, 391 °C with a *dc* bias applied at the same time. The magnitude of the voltage was increased for each measurement cycle, ranging from 0 to 8 V. A comparison of impedance data during voltage application is shown Fig. 3. The three impedance components changed, but not to the same degree. The major change under these conditions occurred at the sample-electrode interface. The Z* plane (a) shows that the low frequency 45° spike collapsed into an arc with resistance R_{el} whose size decreased with increasing voltage until, at 8V, it was visible only as a data point coincident with the low frequency intercept of the grain boundary arc on the Z' axis. The log C' plot (b) shows, with increasing voltage, a reduction in size of the low frequency dispersion, C_{el}, for instance from ~10^{-7} to ~10^{-9} Fcm^{-1} at a frequency of ~0.1 Hz; at

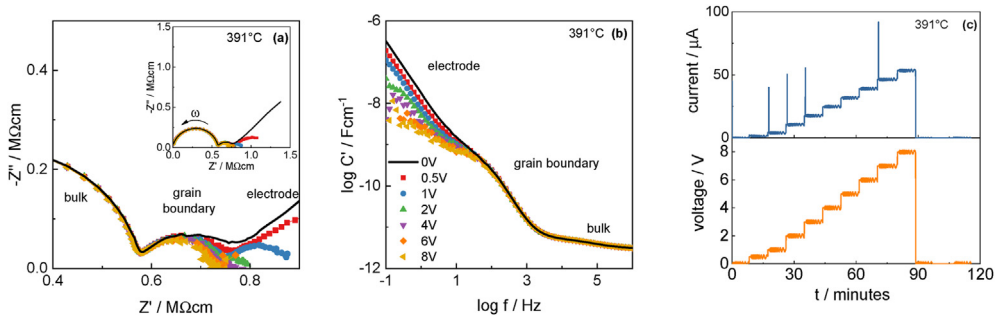

Fig. 3. Change in the impedance response under the application of 0.5–8 V. (a) Impedance complex plane, and (b) spectroscopic plots of capacitance. (c) Current and voltage during impedance measurements. Sample thickness 1.03 mm.

the same time, the data became increasingly noisy.

The changes of the grain boundary response with voltage were not as obvious as those of the electrode response. With increasing voltage, the low frequency intercept of the grain boundary arc on the Z' axis shifted to the left, indicating a decrease of R_{gb}. This change is seen more clearly by comparing the low frequency intercepts of the arc at 0 V (black line) and 8 V (yellow). The log C' plot (b) shows that the capacitance at intermediate frequencies (C_{gb}) did not change by the voltage application.

For the bulk response, the Z* plane (a) shows that the bulk resistance R_b, given by the low frequency intercept of the bulk arc with the Z' axis, remained the same during voltage application. The log C' plot shows that the high frequency response, related to the bulk capacitance, C_b, also remained unchanged.

The current and voltage profiles registered during this sequence of stepwise increase in applied voltage are shown in (c). Of particular note is the current spikes observed on increasing the applied voltage to 1, 2, 3 and 7 V. We attribute the spikes to high fields that are generated initially by each voltage increment at sample-electrode, grain boundary and grain interfaces and surfaces and to the progressive ionisation of layers of O^{2-} ions which extend into the sample interior. The electrons that are liberated in the ionisation processes are responsible for the current spikes and the holes that remain are responsible for the decrease in resistance of the different components.

In summary, with application of up to 8 V during impedance measurements at a temperature near 400 °C, the electrode impedance showed the largest change, followed by a small change to the grain boundary impedance and little or no change to the bulk impedance. This result indicates the introduction of a new current pathway that is initially in parallel with the double layer capacitance C_{el} and allows the current to flow easily across the sample-electrode interface whilst also gradually reducing the resistance of initially, the grain boundaries.

To find out if the changes with *dc* bias were reversible, two impedance measurements were taken after voltage cut off, one immediately after the application of 8 V and the second after a 10 min delay. These measurements are compared to those of the initial state, taken at 0 V before voltage application, in Fig. 4. The grain boundary resistance had recovered the initial state 10 min after voltage cut-off (a) and the capacitance had recovered immediately after voltage cut-off (b). The resistance of the sample-electrode interface, R_{el}, moved towards its initial state value upon removing the voltage, but longer times were required to recover the initial state completely. Accordingly, these results show that the effect of applying up to 8 V during impedance measurements at ~400 °C is, given sufficient time, reversible on removing the bias; although recovery of C_{dl} is very rapid, recovery of R_{gb} takes longer.

3.2. *Intermediate temperatures and voltages: 4.1–16.5 V at 518 °C*

The effect of applying higher voltages for up to 30 min at a higher temperature, ~500 °C was explored. In order to increase the applied voltage, a different impedance analyser was needed and the measuring frequency range changed from 10 Hz to 1 MHz due to instrument limitations. Additional differences from the previous procedure were: (i) voltage was applied for 30 min prior to impedance measurement followed by 30 min of recovery at 0 V before repeat measurements; the cycle was then repeated at higher voltages, (ii) the magnitude of the applied voltage increased in steps from 4.1 to 16.5 V (corresponding to 25 to 100 Vcm^{-1}) and (iii) the temperature was increased to 518 °C. Results are shown in Fig. 5.

The initial response of CSZ at 0 V and 518 °C, given by the black line on the Z* plane Fig. 5(a), shows a decrease in R_b, R_{gb} with increasing field strength and some indication of an accelerated rate of decrease in R_b and R_{gb} at higher voltages. In addition, the electrode spike was much reduced

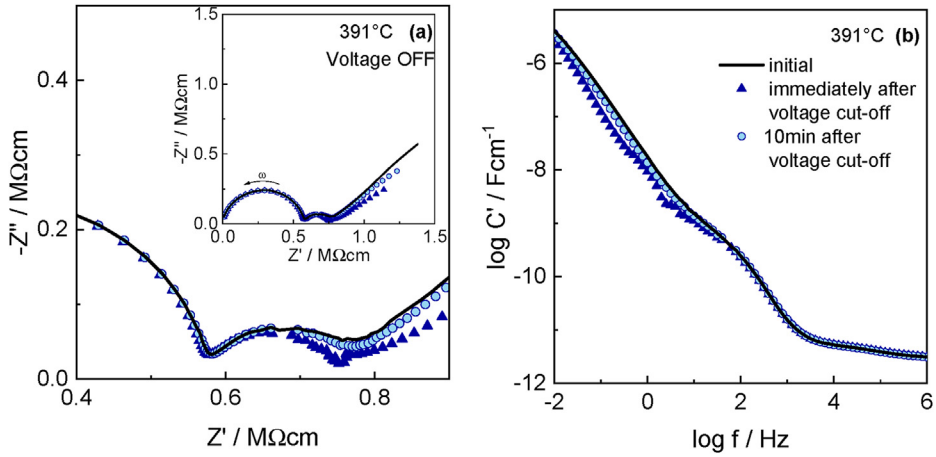

Fig. 4. Impedance response at 391°C at 0 V, before and after application of 8 V, shown in Fig. 3.

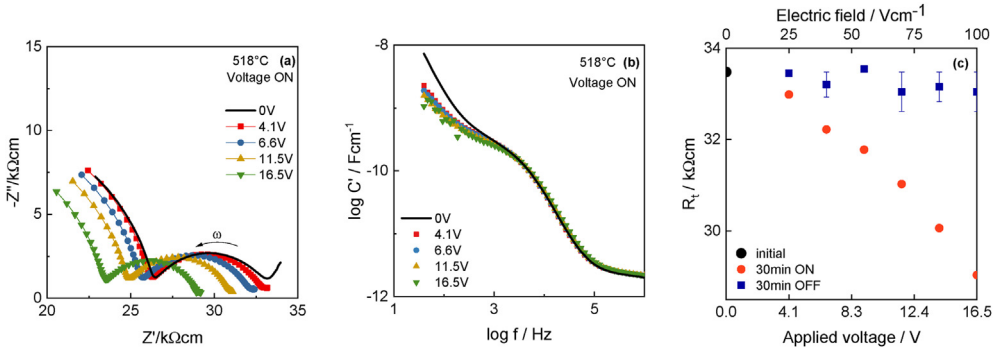

Fig. 5. (a–b) Impedance response at 518°C after 30 min of applied voltage. (c) Total resistance as function of electric field, after 30 min of applied voltage and 30 min after voltage cut off. Sample thickness: 1.65 mm.

in size. C_{el} drops initially on increasing the voltage from 0 to 4.1V (b), while no change was observed in C_b and C_{gb}. The total resistance R_t, given by $R_t = R_b + R_{gb}$, is shown in Fig. 5(c) and confirms an enhanced rate of decrease with increasing voltage. After a recovery time of 30 min from each voltage cut off, R_t had almost recovered its initial state. These results indicate that the voltage-induced changes are still reversible after the application of up to 16.5 V for 30 min at ~500 °C.

The time dependence of the measured impedance, both during voltage application and after its removal at 518 °C, was recorded; the main changes occurred during the first min, as shown for the example of 9.1 V in Fig. 6. The time dependence during voltage application is represented by the "ON" state, (a)-(b); R_t decreased by ~2 kΩcm after 1 min and by an additional ~0.3 kΩcm after 30 min (a). After voltage cut-off, presented as the "OFF" state in (c)-(d), R_t increased from ~31.5 kΩcm to ~32.8 kΩcm during the first min and after 30 min, had recovered the initial value of ~33.2 kΩcm. The log C' (d) plots remained the same after the first minute in both ON and OFF states. These results indicate that application of 4.1 to 16.5 V at ~500 °C had an almost instant effect on the impedance response.

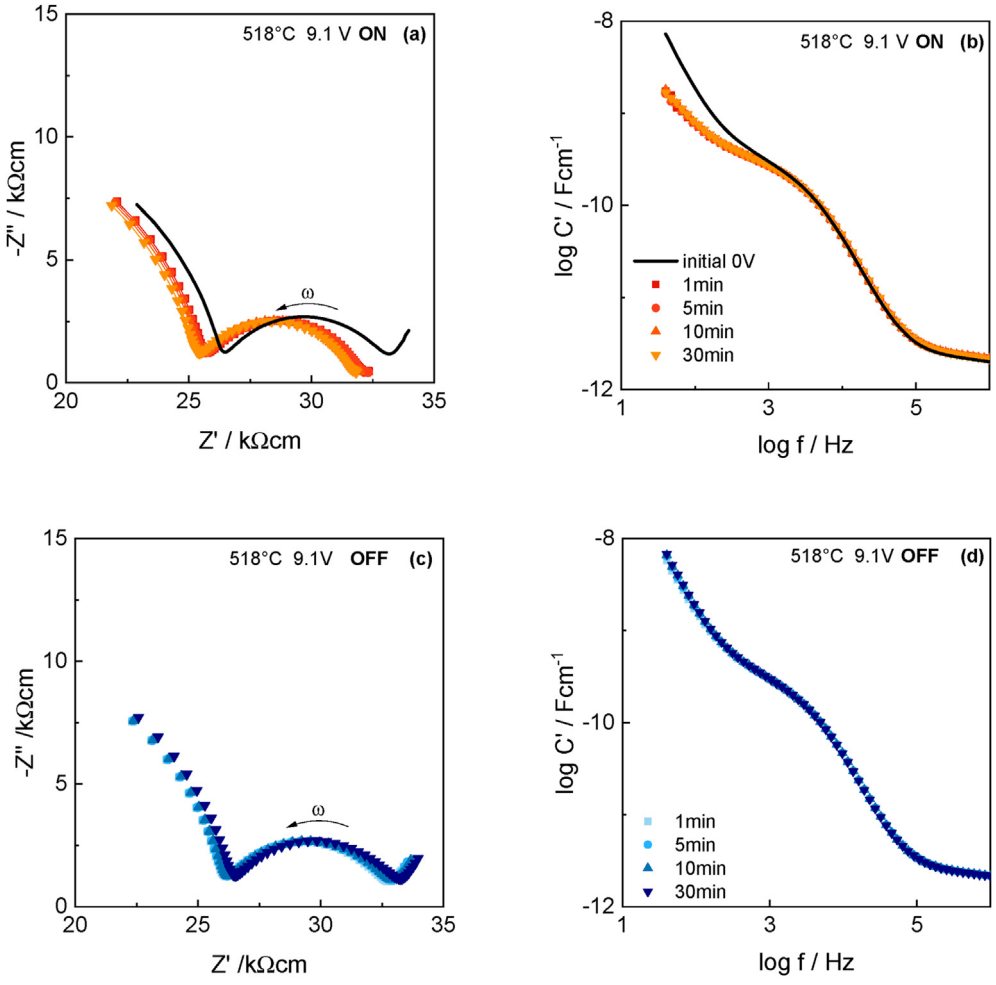

Fig. 6. Time dependence of the impedance response at 518 °C during application (a,b) and removal (c,d) of 9.1 V. Sample thickness: 1.65 mm.

3.3. High temperature and voltages: 600 and 720 °C and 0–25 V; combined effect of pO_2 and voltage

Prior to voltage application at 600 °C, preliminary impedance measurements were taken under different atmospheres with the furnace temperature fixed (T_F) near 600 °C. However, the temperature reading from the thermocouple (T_T) placed near the sample varied by a couple of degrees depending on the purge gas. This might be related to the location of the gas tanks and their exposure to weather conditions and/or to the manual adjustment of the flow rate and gas pressure. To eliminate the variation of T_T prior to voltage application, the initial value of R_t at 0 V for each atmosphere was subtracted from all of the results in that atmosphere to give a normalised difference in R_t, ΔRt, as function of applied voltage. Fig. 7 shows the change in ΔR_t under N_2, dry air and O_2 during the application of 0 to 25 V. The results are essentially independent of pO_2 and show that impedance changes induced by the applied voltage are independent of any atmosphere-sample interactions.

A fresh pellet was used as a sacrificial sample to observe the microstructure near the positive and negative electrodes after applying 25 V for 30 min at 720 °C. Fig. 8 shows SEM micrographs of fracture surfaces and their corresponding EDS maps. The EDS maps showed an even distribution of Zr and minor traces of Ca segregation around some pores, which has also been observed in samples without voltage application [11]. Therefore, no microstructural changes or damage were caused as a consequence of the applied voltage.

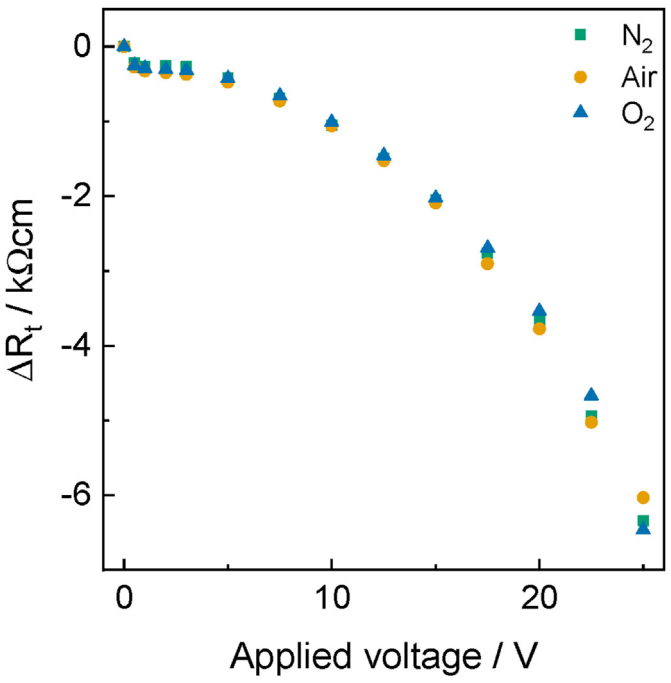

Fig. 7. Difference in the total resistance of CSZ15 with voltage application at ~ 600 °C in N_2, air and O_2. Sample thickness 1.03 mm.

4. Discussion

Composition CSZ15 is an oxide ion conductor under standard conditions, in air at high temperatures [11,15–19]. This paper considers the effect on the electrical properties of an applied voltage in the range 0.5 to 25 V at temperatures in the range 391–600 °C. As previously reported [11], the impedance results showed three main electrical components: the bulk resistance R_b; a grain boundary resistance R_{gb}; a sample-electrode capacitive response that may, or may not have an associated parallel resistance.

The observed voltage effects can be explained in terms of the introduction of *p*-type conduction with holes localised on under-bonded oxygen ions. An under-bonded oxygen refers to an O^{2-} ion that is located either near the sample surface or close to an acceptor dopant. In both such cases, the O^{2-} ion is surrounded by an effective positive charge smaller than 2^+. From electron affinity data, a free O^{2-} ion, in the gas phase, is spontaneously unstable relative to an O^- ion and an electron. An under-bonded O^{2-} ion in a crystal lattice or at a surface or interface may, therefore, either ionise spontaneously under certain circumstances or at least, have a reduced ionisation potential which allows it to ionise in an applied field.

Under mild conditions (0.5–8 V at 391 °C), the sample-electrode response changes rapidly on addition and removal of the bias and is attributed to the introduction of a parallel conduction pathway across the sample-electrode interface. The possibility that the charge transfer resistance associated with the O^{2-}/O_2 reaction becomes very small, allowing resistance-free exchange of oxygen between the ceramic and the gas phase, is considered to be unlikely. Instead, it appears that an electronic conduction pathway was introduced, either by electron injection at the cathode or loss of electrons and hole creation at the anode. It seems unlikely that cathodic reduction of the sample can occur at voltages as small as 0.5 V and therefore, we attribute the creation of electrons to anodic oxidation of oxygen species in an under-bonded environment at the sample surface. The effect of this is to reduce or cancel the double layer capacitance at the sample-anode interface.

Also under mild conditions, the grain boundary resistance decreased with an applied voltage and was recoverable, but more slowly. We attribute this to the oxidation of under-bonded oxygen species located within the grain boundaries. The changes in resistance occur more slowly because of the necessity for diffusion of electrons through the grain boundaries to the ceramic surface.

Under intermediate conditions (up to 16.5 V for 30 min at 518 °C), significant voltage-dependent reduction in R_b was also seen. In this case, we believe that the oxidation of under-bonded oxygen extends into the ceramic bulk. The timescale for this, and its subsequent recovery, is much longer than for the changes seen in the grain boundaries and at the sample-electrode interface.

Since all the changes observed were essentially recoverable on removing the voltage and holding at the same temperature, we do not believe that any irreversible changes, such as decomposition of the sample occurred. Even under harsh conditions (25 V for 30 min at 720 °C), SEM/EDS results, Fig. 8, do not show any evidence of damage to the sample.

It also appears that, since the voltage-induced changes were independent of pO_2, Fig. 7, oxygen exchange reactions between sample and surrounding atmosphere were not the prime cause of the changes. This supports the proposal that voltage-induced ionisation of under-bonded O^{2-} ions was responsible and was detected by enhanced p-type conductivity associated with the O^- ions that acted as location of the holes. We therefore suggest that, in the presence of a *dc* bias, the initial response involves under-bonded oxygen ions that give up an electron at the positive electrode:

$$O_O^x \leftrightarrow O_O^\bullet + e' \quad (1)$$

4.1. Comparison with the literature

Voltage-dependent resistance of CSZ15 ceramics has been observed previously, but without mention of the nature of the electronic charge carriers [20]. The study was performed on symmetrical cells of CSZ15 with oxygen pressures ranging from 1 to 20 atm and application of voltages from 0 to 6 V at 560 °C. The results showed two regimes, attributed to different rate-limiting steps [20]. Below 2 V, the resistance varied with pO_2 and was associated with oxygen diffusion through the Pt electrode. Above 2 V, no pO_2 dependence was observed.

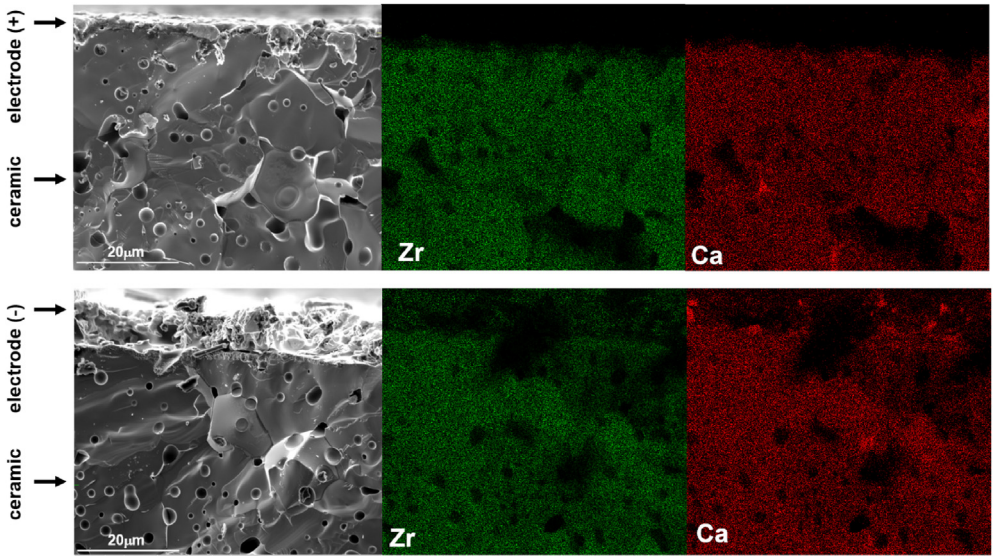

Fig. 8. *Micrographs of fracture surface near the electrodes after being subjected to 25 V for* 30 min *at 720 °C* [14].

The results presented here are similar in many respects to those reported for YSZ [3,9,10]. Composition YSZ8 showed the onset of electronic conductivity with an applied bias [10], whereas compositions with a higher yttria content showed sensitivity to both pO_2 and *dc* bias [3]; at low bias, the pO_2-dependence confirmed the mechanism to be *p*-type [8].

The occurrence of *p*-type conductivity with electron holes on O^- ions as charge carriers has been suggested also for Mg-doped alumina [21–24], $SrTiO_3$ [25] and Mg-, Zn- and Ca-doped $BaTiO_3$ ceramics [5–7]. For the doped $BaTiO_3$ systems, time-dependent impedance measurements showed the growth of a second M'' peak, which was attributed to the nucleation of a more conductive new phase, which initiated at the anode surface and extended into the sample interior as the *p*-type layer grew thicker.

5. Conclusions

$Ca_{0.15}Zr_{0.85}O_{1.85}$ ceramic is an oxide ion conductor under standard atmospheric conditions but becomes a mixed conductor due to the introduction of *p*-type semi-conductivity on application of a small bias voltage at high temperatures. Three stages were detected, depending on temperature, time and magnitude of the applied voltage. The first stage involved rapid electron transfer across the sample-electrode interface which acted to short-circuit the double layer capacitance associated with oxide ion accumulation/depletion at the sample surfaces. The source of the electrons is attributed to ionisation of under-bonded oxide ions at the anode surface. On removal of the bias, the double layer electrode capacitance recovered rapidly.

In the second stage, the grain boundary resistance started to decrease and was subsequently recovered, but more slowly, on removal of the bias. The resistance decrease was attributed to hole creation by ionisation of under-bonded oxide ions within the grain boundary regions. A similar effect was seen in the third stage but now involving the ceramic grains; it occurred only at higher temperatures and had a longer recovery time after removal of the bias. The conductivity changes were time-dependent, especially those involving sample grains, and were attributed to the long range diffusion of electrons between sample interior and the surface. There was no evidence of sample degradation, even at the highest voltage and temperature.

The voltage-induced changes were not influenced by pO_2 in the surrounding atmosphere and therefore, were not controlled by oxygen exchange reactions at the gas-solid interfaces. They occurred with a bias voltage as low as 0.5 V; consequently, the resistance decrease is not attributed to electron injection at the cathode interface but to hole creation at the anode interface.

These results show that composition CSZ15 is close to the upper pO_2 limit of its electrolytic domain and to the cross-over between oxide ion conduction and *p*-type semi-conduction.

Declaration of competing interest

The authors declare that they have no known competing financial interests or personal relationships that could have appeared to influence the work reported in this paper.

Acknowledgments

JRG thanks CONACyT for a studentship, grant number 578893/409341 and the EPSRC, award reference 1880882.

References

[1] F. Hund, Die Fluoritphase im System ZrO_2-CaO, Z. Phys. Chem. 199 (1) (1952) 142.
[2] F.A. Kröger, "Electronic conductivity of calcia-stabilized zirconia, J. Am. Ceram. Soc. 49 (4) (1966) 215–218.
[3] M. Jovaní, H. Beltrán-Mir, E. Cordoncillo, A.R. West, Atmosphere- and voltage-dependent electronic conductivity of oxide-ion-conducting $Zr_{1-x}Y_xO_{2-x/2}$ ceramics, Inorg. Chem. 56 (12) (2017) 7081–7088.
[4] T.B. Adams, D.C. Sinclair, A.R. West, Characterization of grain boundary impedances in fine- and coarse-grained $CaCu_3Ti_4O_{12}$ ceramics, Phys. Rev. B Condens. Matter 73 (9) (2006) 1–9.
[5] M. Prades, N. Masó, H. Beltrán, E. Cordoncillo, A.R. West, "Field enhanced bulk conductivity of $BaTiO_3$: Mg ceramics, J. Mater. Chem. 20 (25) (2010) 5335.
[6] H. Beltrán, M. Prades, N. Masó, E. Cordoncillo, A.R. West, Voltage-dependent low-field bulk resistivity in $BaTiO_3$:Zn ceramics, J. Am. Ceram. Soc. 93 (2) (2010) 500–505.
[7] N. Masó, M. Prades, H. Beltrán, E. Cordoncillo, D.C. Sinclair, A.R. West, Field enhanced bulk conductivity of acceptor-doped $BaTi_{1-x}Ca_xO_{3-x}$ ceramics, Appl. Phys. Lett. 97 (6) (2010) 5335–5344.
[8] M. Jovaní, H. Beltrán-Mir, E. Cordoncillo, A.R. West, Field-induced p-n transition in yttria-stabilized zirconia, Sci. Rep. 9 (2019).
[9] X. Vendrell, A.R. West, Induced p-type semiconductivity in yttria-stabilized zirconia, J. Am. Ceram. Soc. 102 (10) (Oct. 2019) 6100–6106.
[10] N. Masó, A.R. West, Electronic conductivity in Yttria-stabilized zirconia under a small dc bias, Chem. Mater. 27 (5) (2015) 1552–1558.
[11] J. Ramírez-González, A.R. West, Electrical properties of calcia-stabilised zirconia ceramics, J. Eur. Ceram. Soc. 40 (2020) 5602–5611.
[12] S.Y. Kwon, I.H. Jung, Critical evaluation and thermodynamic optimization of the CaO-ZrO2 and SiO2-ZrO2 systems, J. Eur. Ceram. Soc. 37 (3) (2017) 1105–1116.
[13] B.A. Boukamp, B.A. van Hassel, I.C. Vinke, K.J. De Vries, A.J. Burggraaf, The oxygen transfer process on solid oxide/noble metal electrodes, studied with impedance spectroscopy, dc polarization and isotope exchange, Electrochim. Acta 38 (14) (1993) 1817–1825.

[14] J. Ramírez-González, PhD Thesis, "Synthesis and Electrical Characterization of Calcia-Stabilised Zirconia and Mg-Doped Alumina, " The University of Sheffield, 2020.
[15] T.H. Etsell, S.N. Flengas, The electrical properties of solid oxide electrolytes, Chem. Rev. 70 (3) (1970) 339–376.
[16] A. Nakamura, J.B. Wagner, Defect structure, ionic conductivity, and diffusion in calcia-stabilized zirconia, J. Electrochem. Soc. 127 (11) (1980) 2325–2333.
[17] S. Jing-ze, W. Yu-ming, Diffusion in fast-ion conductor calcia-stabilized zirconia: a molecular dynamics study, Chin. Phys. Lett. 15 (10) (1998) 727.
[18] S. Kazlauskas, A. Kežionis, T. Šalkus, A.F. Orliukas, Electrical properties of YSZ and CaSZ single crystals, Solid State Ionics 231 (2013) 37–42.
[19] O.Y. Kurapova, O. V Glumov, M.M. Pivovarov, S.N. Golubev, V.G. Konakov, Structure and conductivity of calcia stabilized zirconia ceramics, manufactured from freeze-dried nanopowder, Rev. Adv. Mater. Sci. 52 (1–2) (2017) 134–141.
[20] H. Yanagida, R.J. Brook, F.A. Kröger, Direct current-voltage characteristics of calcia stabilized zirconia with porous platinum electrodes, J. Electrochem. Soc. 117 (5) (1970) 593.
[21] S.K. Mohapatra, F.A. Kröger, "Defect structure of α-Al2O_3 doped with magnesium, J. Am. Ceram. Soc. 60 (3–4) (1977) 141–148.
[22] F.T. Gamble, R.H. Bartram, C.G. Young, O.R. Gilliam, P.W. Levy, Electron-spin resonances in gamma-ray-irradiated aluminum oxide, Phys. Rev. 134 (3A) (1964).
[23] R.H. Bartram, C.E. Swenberg, J.T. Fournier, Theory of trapped-hole centers in aluminum oxide, Phys. Rev. 139 (3A) (1965) A941–A951.
[24] J. Kvapil, B. Perner, J. Súlovský, J. Kvapil, Colour centre formation in corundum doped with divalent ions, Krist. Tech. 8 (1–3) (1973) 247–251.
[25] K. Klauke, et al., Enhancement of the $SrTiO_3$ surface reactivity by exposure to electric fields, ChemNanoMat 5 (7) (2019) 948–956.